Extended rift-associated volcanism in Ganis Chasma, Venus detected from Magellan radar emissivity

J. Brossier[1]*, M.S. Gilmore[2], J.W. Head[3]

(1) Institute for Space Astrophysics and Planetology IAPS, National Institute of Astrophysics, 100 Via del Fosso del Cavaliere, 00133 Rome, Italy

(2) Wesleyan University, Department of Earth and Environmental Sciences, Planetary Sciences Group, 265 Church Street, Middletown, CT 06459, USA

(3) Brown University, Department of Earth, Environmental and Planetary Sciences, 324 Brook Street, Providence, RI 02912, USA

*Corresponding author: Jeremy Brossier (brossier.jrmy@gmail.com)

Keywords: Venus, Magellan, Rifts, Mineralogy, Age, Ganis Chasma

Key Points [up to 3 points, 140 characters]

1. Radar anomalies in Ganis Chasma correspond to transient bright spots seen in infrared data
2. Low radar emissivity values suggest recent volcanic and tectonic activity on Venus
3. Lava flows in Ganis Chasma may have erupted over the last 30 years

Abstract (140 words – max 150!)

Exploration of Venus in the 1970–1990's revealed that the geology of Venus, the most Earth-like of the terrestrial planets, was decidedly un-Earth-like, with no plate tectonics, and no record of the first 80% of its history. A major outstanding question is whether Venus is still volcanically active today. We find that regions of Ganis Chasma have low radar emissivity values, due to low volumes of high dielectric minerals formed by surface – atmosphere weathering on the timescales of around 10s Ma. This confirms the presence of geologically recent volcanism in association with this major tectonic rift zone. The spatial correspondence of this emissivity signature with transient thermal anomalies suggests that Venus has been volcanically active at this site for at least the last few decades, a prediction that can be tested with space missions to Venus in the coming decade.

1 ONGOING VOLCANISM ON VENUS?

The diameter of Venus predicts that it should, like Earth, be volcanically active today (e.g., Head and Solomon, 1981). Radar images of the surface collected during the Magellan mission (1990–1994) did not identify any morphological evidence of volcanic activity. Nonetheless, recent and ongoing volcanic activity on Venus is suggested by other multiple independent lines of evidence. Pioneer Venus Orbiter (PV, 1978–1986) and Venus Express (VEx, 2005–2014) missions gathered more than 30 years of atmospheric measurements searching for evidence of possible volcanic eruptions. Both missions revealed fluctuations in sulfur dioxide (SO_2) that are possibly associated with volcanic outgassing on Venus (e.g., Esposito, 1984; Esposito et al., 1988; Marcq et al., 2012).

Idunn Mons, located in Imdr Regio, is considered to be among the most likely sites for active volcanism on the planet. Smrekar et al. (2010) detected some lava flows with relatively high thermal emission at 1 μm in the region. Infrared (1-μm) emissivity is derived from the Visual and Infrared Thermal Imaging Spectrometer (VIRTIS) images of the southern hemisphere returned by the VEx mission (Helbert et al., 2008; Mueller et al., 2008). In their work, Smrekar et al. (2010) suggest that the surface of Idunn Mons is made of young and unweathered lava flows, and hence, the volcano was possibly still active. Further investigations at Idunn reported that the young lava flows are more likely found on the eastern flanks of the volcano (D'Incecco et al., 2017), and contemporaneous to stratigraphically young structures associated with rifting at Olapa Chasma (D'Incecco et al., 2020; López et al., 2022). Other regions show a higher 1-μm emissivity relative to the surrounding plains, notably Hathor and Innini montes in Dione Regio (Mueller et al., 2008),

Mielikki Mons, Shulamite and Shiwanokia coronae in Themis Regio (Stofan et al., 2009, 2016). The ages of the fresh, basaltic lava flows could not be well constrained since the timescale for chemical weathering in the near-surface environment of Venus is fundamentally unknown. The VIRTIS 1-µm emissivity data are expected to be controlled by the oxidation of ferrous iron in basalts to hematite, where the high thermal emission of Idunn Mons is thought to represent lower degrees of weathering; Smrekar et al. (2010) estimate that the volcano is 2.5 million years old or younger based on this reaction. More recent experimental studies under Venus conditions (Berger et al., 2019; Cutler et al., 2020; Filiberto et al., 2020; Teffeteller et al., 2022) suggest that chemical weathering occurs on much shorter time frames (i.e., in weeks to months).

Atla Regio is another region of prime interest for ongoing volcanic and tectonic activity, which is supported by analysis of the gravity and altimetry data returned by Magellan (Phillips, 1994; Smrekar, 1994; Stofan et al., 1995), and thermal anomalies observed by the Venus Monitoring Camera (VMC) during the VEx mission (Shalygin et al., 2012; 2015). Additionally, several analyses based on stratigraphic relationships between rift structures, lava flows, and crater features provide further evidence for the relative youthfulness of the region (e.g., Basilevsky, 1993; Basilevsky and Head, 2002a; 2002b; Brossier et al., 2021). VMC data collected during 2007–2009 did not reveal any signs of ongoing volcanic eruptions for the major volcanoes in Atla Regio (i.e., Maat, Ozza and Sapas montes) (Shalygin et al., 2012). However, they show several suspicious high (1-µm) emission spots near Ganis Chasma that varied in location and intensity over several days to months (Shalygin et al., 2015). Ganis Chasma (or Ganiki Chasma) is a rift zone in Atla Regio centered at 192°E, 18°N, where recent activity was already suggested based on the superposition of rift structures on young impact deposits (Basilevsky, 1993). Shalygin et al. (2015) propose that these transient high emission spots are consistent with short-lived effusive activity, locally causing significant increases of surface temperatures.

2 MAGELLAN EMISSIVITY AS A CHRONOMETER

Radar emissivity can also be used as proxy to constrain the degree of weathering and therefore surface age of volcanic systems. Pioneer Venus and Magellan data show that many of Venus's highlands have distinctly elevated values of radar reflectivity (Masursky et al., 1980; Ford and Pettengill, 1983) and thus low values of radar emissivity at their summits (Pettengill et al., 1992). These radar "anomalies" are ascribed to the presence of minerals with a high dielectric constant.

Indeed, it is expected from theory that materials with high dielectric constants will enhance their radar reflectivity and lower their radar emissivity (Pettengill et al., 1992; Campbell, 1994). Several studies indicate that high dielectric minerals can be produced through chemical weathering reactions between the rocks and the near-surface atmosphere (e.g., Klose et al., 1992; Schaefer and Fegley, 2004; Treiman et al., 2016; Semprich et al., 2020 and references therein); if so, the reduction in radar emissivity can be associated with the formation of high dielectric minerals over time and thus can serve as a chronometer.

Brossier et al. (2020) reveal that most volcanoes and coronae on Venus are compatible with the presence of ferroelectric minerals in their rocks, particularly the tallest volcanoes on the planet (~~e.g.,~~ Maat and Ozza montes). Ferroelectric minerals (e.g., chlorapatite, perovskite oxides) are substances that undergo a phase transition when they reach a certain temperature, also **called** the Curie temperature, where its dielectric constant increases strongly. As the temperature rises above the Curie temperature (i.e., lower elevation on Venus), its dielectric constant gradually declines to normal values (Shepard et al., 1994; Treiman et al., 2016). Elevation and shape of the emissivity variations described in Brossier et al. (2020) indicate the presence of ferroelectrics with Curie temperatures of 693–731 K over a range of elevation between 6052.5 km and 6056.7 km. The varying "critical altitudes" reported in Klose et al. (1992) and seen by Brossier and colleagues could be due to diverse mineralogical compositions, or local differences in the atmospheric composition or temperature (Treiman et al., 2016). A more detailed investigation in Atla Regio (Brossier et al., 2021), shows that Maat and Ozza montes display multiple reductions in radar emissivity at different altitudes including, atypically, lowlands. They reported that these low emissivity signatures are found to correlate with individual lava flows, indicating that the excursions are controlled by variations in rock chemistry as opposed to the deposition of atmospheric precipitates.

Here we extract radar emissivity and elevation data collected during the Magellan mission (1990–1994) and examine the variation of emissivity with altitude for sites at Ganis Chasma identified as thermal anomalies in the VMC data (Shalygin et al., 2015), thus providing an independent constraint on surface age in the region. We believe that a detailed description of the radiophysical behaviors of these sites may help to retrieve, or at least constrain, their relative age and composition (as in Brossier et al., 2020; 2021; Brossier and Gilmore, 2021). The present paper is therefore

organized as follows. We first locate and describe the changes in radar emissivity with altitude for the selected sites of interest in order to assess in detail the radiophysical signatures seen in Ganis Chasma (Section 4). This aims to determine whether the material measured in the region has the behavior consistent with that of known substances and we consider whether emissivity variations are related to rock age (Section 5).

3 DATA & METHODS

Our investigation uses radar datasets compiled during the Magellan mission (frequency = 2.4 GHz, λ = 12 cm). Morphological units are identified with the Cycle 1 left-looking Magellan Synthetic Aperture Radar (SAR) images (FMAPS) produced at a resolution of 75 m per pixel. The rift valley as well as the surrounding craters (e.g., Sitwell and Bashkirtseff craters), volcanoes (e.g., Yolkai-Estsan Mons) and tesserae were initially mapped in Ivanov and Head (2011) (Figure 1).

[Figure 1]

We derived altimetry and emissivity from the Magellan global topography data records (GTDR) and global emissivity data records (GEDR). Altimetry data have a spatial resolution ranging from ~10 km at periapsis (ca. 10˚N latitude) to ~20 km near the poles (ca. 90˚N and 70˚S) when the orbiting spacecraft was high above the planet. Emissivity data were collected while the spacecraft was operating in radiometer mode. The spatial resolution of the emissivity data varies from ~20 km near periapsis to ~80 km at high latitudes (Pettengill et al., 1991). Near-global mosaics are produced in the GTDR and GEDR data products that are publicly available through the USGS websites (https://planetarymaps.usgs.gov/mosaic). The two mosaics are resampled to a spatial resolution of 4.6 km per pixel (scale of 22.7 pixel per degree). Altimetry and emissivity data are extracted from these mosaics to produce scatterplots of the emissivity variation with altitude for each site of interest (e.g., Brossier et al., 2020; Brossier and Gilmore, 2021; Brossier et al., 2021), as in Klose et al. (1992). Elevation data are given in planetary radius with a mean value taken as 6051.8 km (Ford and Pettengill, 1992). Selection and extraction processes are done with the ArcGIS 10.6 (ESRI) software package, while the plots are produced with RStudio software. We also retrieve temperatures by correlation to the Vega 2 lander entry profile (Seiff, 1987; Lorenz et al., 2018; Brossier et al., 2020). Magellan datasets covering the study area, shapefiles (mapped

136 units, and sites of interest), and extracted values (emissivity, altimetry and temperatures) are
137 available through the online repository linked to this work (Brossier et al. 2022).

138 [Figure 2]

139 **4 RESULTS**

140 **4.1 Study Sites**

141 Our extraction is performed on the four sites studied with VMC data in Shalygin et al. (2015) (sites
142 1–4), and three other sites (sites 5–7) for comparison purposes. Figure 1 displays the major
143 morphological features in the region, while Figure 2 indicates the emissivity and elevation
144 variations for each site. Sites 1 and 4 are located at the margins of the rift valley, and replicate the
145 boundaries of the strongest thermal anomalies identified by Shalygin et al. (2015). Both sites
146 comprise outer flows and faulted walls of the rift valley. Sites 2 and 3 are also considered as areas
147 of recent activity, and correspond to high elevated and faulted walls of the rift valley. Among the
148 new sites, 5 and 6 are morphologically similar to sites 2 and 3, and at similar high elevations. Site
149 7 corresponds to the extensive lava flows of Yolkai-Estsan Mons (hereafter called Yolkai for
150 simplicity). This volcano has been heavily dissected by faults and is thus older than the rifting.
151 Sitwell crater (32.8 km–diameter) has a parabolic ejecta deposit (parabola) that is superimposed
152 on Ganis Chasma, and may have undergone some rift-associated fracturing. This indicates possible
153 continuation of rifting activity in this part of Ganis Chasma after the formation of the crater and
154 its parabola (Basilevsky, 1993). Bashkirtseff crater (36.3 km–diameter) is another crater in the
155 region that lacks a parabola and appears to be embayed by Yolkai lava flows.

156 **4.2 Emissivity Excursions**

157 Figure 3A shows elevation – emissivity plots obtained for the seven sites of interest. Because both
158 composition and surface roughness can reduce emissivity, we distinguish emissivity values
159 derived from the faulted walls of Ganis Chasma (red dots), from those related to flow materials at
160 the edge of the rift (black dots) (see also Figure S1). Nonetheless, it is worth noting that this
161 distinction may include some surrounding effects due to the difference in resolutions between SAR
162 images (75 m per pixel) for the mapping of the lava flows and faulted walls, and the extraction of
163 the elevation and emissivity data (4.6 km per pixel).

The magnitude of an emissivity excursion is defined by the percentage decrease between the minimum emissivity value observed in a region and the planetary average of ~0.85. We observe different magnitudes and behaviors of the emissivity excursions: (1) a "strong" excursion is where emissivity shows a decrease of ~30% or more from the planetary average value, (2) a "subtle" excursion shows a decrease of 10–30%, or (3) no changes (≤ 10%) where emissivity is nearly constant with elevation. Figure 3B reports the magnitude of the emissivity excursions detected in each site and the corresponding altitude and temperature. Excursion magnitudes reported here are those of the lava flow units (black dots in Figure 3A), mitigating surface roughness effects. Sites 1–4 and site 6 have subtle declines in emissivity that reach low values of 0.672–0.753 at altitudes varying between 6054.2 km and 6055.8 km (701–716 K). Conversely, sites 5 and 7 have strong declines to values of 0.595–0.600 reached at 6056.2 km (697 K) and 6054.5 km (713 K), respectively. All values are summarized in Table 1 for all sites of interest.

[Figure 3]

[Table 1]

5 COMPOSITION & RELATIVE AGE

At each site, emissivity values gradually decline with increasing altitude from the lowlands (i.e., below 6053 km) to a given elevation (Figure 3A). This pattern of emissivity variations with altitude is consistent with ferroelectric behavior, characterized by a steady, gradual decline in radar emissivity with increasing elevation, then a sharp return to higher emissivity values at altitudes above 6056 km (around 700 K). Such a behavior is observed in Ovda Regio (Shepard et al., 1994; Treiman et al., 2016) and more globally in most volcanic edifices and tesserae on the planet (Brossier et al., 2020; Brossier and Gilmore, 2021). Ferroelectric minerals are known to be very conductive at a certain temperature, namely the mineral's Curie temperature (Tc). In Ganis Chasma, we see this behavior for site 1 (Figure 3A), and although the other sites do not reach elevations of 6056 km, the shape of the emissivity – elevation curve is similar to site 1 and other examples of ferroelectric behavior (Shepard et al., 1994; Treiman et al., 2016; Brossier et al., 2020; Brossier and Gilmore, 2021). In the ferroelectric model, the altitude (and temperature) of an emissivity excursion is a function of the composition, while its magnitude is a function of the volume of ferroelectric minerals (Shepard et al., 1994; Brossier et al., 2021). Chlorapatite and some perovskite oxides are good candidates, as their transition from ferro- to paraelectric occurs

194 at temperatures found on the surface of Venus (690–735 K). The reader is referred to Brossier et
195 al. (2021) for more details on the presence of ferroelectrics on Venus.

196 To use emissivity as a chronometer, we assume that the lava flows have a similar initial
197 composition, and that the primary minerals in the flows are chemically weathered by the
198 atmosphere over time to produce secondary minerals with high dielectric constants. In this model,
199 sites with strong emissivity excursions occurring at high altitude (above 6053 km) are thought to
200 have had enough time to produce the ferroelectric minerals responsible for the radar anomalies in
201 the region via surface – atmosphere chemical weathering reactions. Conversely, sites with subtle
202 or no emissivity excursions at high altitudes are considered to be young or possibly active since
203 they have a lower volume of ferroelectric minerals. This model is supported by studies of other
204 large volcanoes, such as Maat, Idunn and Otafuku montes, whose lava flows show subtle to low
205 emissivity excursions that correlate with recent stratigraphic position (Brossier et al., 2020; 2021).
206 In Ganis Chasma, the emissivity patterns imply that the youngest features are in sites 1, 3 and 4
207 (subtle to no emissivity excursions), while the oldest features are in sites 5 and 7 (strong emissivity
208 excursions). This interpretation is in good agreement with the observations made using VMC
209 images by Shalygin et al. (2015). In Ganis Chasma (and other rift valleys), rifting process may
210 have an important role in faulting and creating freshly exposed rocks, and it would produce a
211 signature similar to the newly erupted lava flows. Indeed, ferroelectric minerals would be formed
212 or "triggered" in contact with the near-surface environment; thus, these detections may indicate
213 the presence of very recent tectonic activity, in concert with the associate evidence for recent
214 volcanism.

215 Shalygin et al. (2015) report that site 1 was the most prominent spot, followed by sites 2 and 3,
216 while at site 4 it was uncertain if it was transient. It is worth noting that the IR-bright spots from
217 VMC data are short-lived (only lasted a few days) and observed in 2008–2009. Conversely, our
218 analysis displays older signatures from the early 1990's, leading to a 20 year-gap between the two
219 observations. This suggests that site 2 has erupted since it was imaged by Magellan.

220 Overall, the sites have similar emissivity behaviors (variation with altitude) at comparable
221 elevation ranges (Figure 3A), although they present different excursion magnitudes (i.e., different
222 volume, age) and slightly different critical altitude (i.e., temperature, composition) (Figure 3B).
223 Site 6 is uncertain since the data points are more diffuse. Interestingly, site 7 has a distinct

emissivity pattern, with a strong excursion at low elevation (below 6055 km) that resemble that of some volcanoes on Venus, such as Sekmet and Anala montes (Brossier et al., 2020). This slight variability in critical altitudes could be ascribed to slight differences in the ferroelectric composition, as discussed in Shepard et al. (1994) and Treiman et al. (2016). Shepard et al. (1994) demonstrate that minor change of the Pb abundance in a (Pb,Ca)TiO_3 perovskite can increase or decrease the Curie temperature (Rupprecht and Bell, 1964), and hence the critical altitude. For instance, a 1% change in the Pb abundance changes the Curie temperature by ~8 K, corresponding to a 1 km change in the transition altitude. Treiman et al. (2016) suggests that differences in anion composition (OH, F and Cl) or cation composition (substitution of Sr or rare Earth elements for Ca) in a $Ca_5(PO_4)_3$(OH,F,Cl) apatite can also change the Curie temperature. More importantly, they state that chlorapatite is ferroelectric and thus the F:Cl ratio will control the Curie temperature where apatite with a larger F:Cl ratio would require higher temperatures (i.e., lower elevations) to exhibit a high dielectric constant (Rausch, 1976).

6 CONCLUSION

We show that the transient IR-bright spots detected in Shalygin et al. (2015) have radar emissivity values close to the planetary average (~0.85). Other regions in Ganis Chasma with similar morphology and elevation range have low emissivity values indicating the presence of minerals with a high dielectric constant (e.g., ferroelectrics), predicted to be produced by chemical weathering over time.

Sites 1, 3 and 4 are characterized by young materials, as they lack minerals with high dielectric constant (not yet produced). Sites 5 and 7 are characterized by older materials with a greater volume of these minerals. This is further supported for site 7 that has been dissected by the rift formation. All sites are consistent with the presence of ferroelectrics with subtle differences in the mineral composition (chlorapatite, or perovskite oxides). This is in agreement with the other volcanoes in Atla Regio, Maat and Ozza montes (Brossier et al., 2020; Brossier et al., 2021). The pattern of the radar emissivity in these regions is consistent with relatively young and unweathered materials. The transient IR-bright spots in these regions detected 20 years after Magellan, provide independent corroboration of active volcanism in Ganis Chasma since the 1990's.

As a possible site of current tectonic and volcanic activity, Atla Regio represents one important science target for the upcoming missions to Venus. NASA's Venus Emissivity, Radio Science,

InSAR, Topography & Spectroscopy (VERITAS) mission (Smrekar et al., 2020) and ESA's EnVision mission (Ghail et al., 2012, 2020) would return complementary, critical datasets including improved topography, SAR imaging, gravity, and infrared spectroscopy.

Acknowledgments

This research has been carried out at Wesleyan University and supported by NASA Solar System Workings [grant 80NSSC19K0549] to MSG. We greatly acknowledge the teams responsible for the Magellan datasets accessible via the USGS website (https://planetarymaps.usgs.gov/mosaic).

Data Availability Statement

All data used in our mapping and plotting procedures (e.g., Magellan images, shapefiles and extracted values for the sites of interest) can be found in the online repository linked to this study (Brossier et al. 2022). Magellan global datasets are also provided through the USGS website (https://planetarymaps.usgs.gov/mosaic), and described in Ford et al. (1993).

References

Basilevsky, A.T. (1993). Age of rifting and associated volcanism in Atla Regio, Venus. GRL 20, 883–886. https://doi.org/10.1029/93GL00736

Berger, G., et al. (2019). Experimental exploration of volcanic rocks atmosphere interaction under Venus surface conditions. Icarus 329, 8–23. https://doi.org/10.1016/j.icarus.2019.03.033

Brossier, J., Gilmore, M.S., and Toner, K. (2020). Low radar emissivity signatures on Venus volcanoes and coronae: New insights on relative composition and age. Icarus 343, 113693. https://doi.org/10.1016/j.icarus.2020.113693

Brossier, J., and Gilmore, M.S. (2021). Variations in the radiophysical properties of tesserae and mountain belts on Venus: Classification and mineralogical trends. Icarus, 114161. https://doi.org/10.1016/j.icarus.2020.114161

Brossier, J., Gilmore, M.S., Toner, K., and Stein, A.J. (2021). Distinct mineralogy and age of individual lava flows in Atla Regio, Venus derived from Magellan radar emissivity. JGR 126, e2020JE006722. https://doi.org/10.1029/2020JE006722

Brossier, J., Gilmore, M.S., and Head, J.W. (2022). Possible recent or current rift-associated volcanism in Ganis Chasma, Venus: Supporting datasets. https://doi.org/10.6084/m9.figshare.18901715

Cutler, K.S., Filiberto, J., Treiman, A.H., and Trang, D. (2020). Experimental investigation of oxidation of pyroxene and basalt: implications for spectroscopic analyses of the surface of Venus and the ages of lava flows. PSJ 1:21, 10pp. https://doi.org/10.3847/psj/ab8faf

D'Incecco, P., Müller, N., and D'Amore, M. (2017). Idunn Mons on Venus: Location and extent of recently active lava flows. PSS 136, 25–33. http://dx.doi.org/10.1016/j.pss.2016.12.002

D'Incecco, P., et al. (2020). Local stratigraphic relations at Sandel crater, Venus: Possible evidence for recent volcano-tectonic activity in Imdr Regio. EPSL 546, 116410. https://doi.org/10.1016/j.epsl.2020.116410

Esposito, L.W. (1984). Sulfur dioxide – Episodic injection shows evidence for active Venus volcanism. Science 223, 1072–1074. https://doi.org/10.1126/science.223.4640.1072

Esposito, L.W., et al. (1988). Sulfur dioxide at the Venus cloud tops, 1978–1986. JGR 93, 5267–5276. https://doi.org/10.1029/JD093iD05p05267

Filiberto, J., Trang, D., Treiman, A.H., Gilmore, M.S. (2020). Present-day volcanism on Venus as evidenced from weathering rates of olivine. Science Advances 6(1), https://doi.org/10.1126/sciadv.aax7445

Ford, J.P., et al. (1993). Guide to Magellan Image Interpretation. JPL Publication 93–24, 1-18. https://ntrs.nasa.gov/archive/nasa/casi.ntrs.nasa.gov/19940013181.pdf

Ford, P.G., and Pettengill, G.H. (1992). Venus topography and kilometer-scale slopes. JGR 97, 13103–13114. https://doi.org/10.1029/92JE01085

Ghail, R.C., et al. (2020). The science goals of the EnVision Venus orbiter mission. 15th EPSC Abstracts, EPSC2020–599. https://doi.org/10.5194/epsc2020-599

Ghail, R.C., et al. (2012). EnVision: Taking the pulse of our twin planet. Experimental Astronomy, 33(2), 337–363. https://doi.org/10.1007/s10686-011-9244-3

306 Head, J.W., and Solomon, S.C. (1981). Tectonic evolution of the terrestrial planets. Science 213,
307 62–76. https://doi.org/10.1126/science.213.4503.62

308 Helbert, J., et al. (2008). Surface brightness variations seen by VIRTIS on Venus Express and
309 implications for the evolution of the Lada Terra Region, Venus. GRL 35, L11201.
310 https://doi.org/10.1029/2008GL033609

311 Ivanov, M.A., and Head, J.W. (2011). Global geological map of Venus. PSS 59, 1559–1600.
312 https://doi.org/10.1016/j.pss.2011.07.008

313 Klose, K.B., Wood, J.A., and Hashimoto, A. (1992). Mineral equilibria and the high radar
314 reflectivity of Venus mountaintops. JGR 97, 16353–16369. https://doi.org/10.1029/92JE01865

315 López, I., D'Incecco, P., Filiberto, J., and Komatsu, G. (2022). The volcanology of Idunn Mons,
316 Venus: The complex evolution of a possible active volcano. Journal of Volcanology and
317 Geothermal Research 421, 107428. https://doi.org/10.1016/j.jvolgeores.2021.107428

318 Lorenz, R.D., Crisp, D., and Huber, L. (2018). Venus atmospheric structure and dynamics from
319 the VEGA lander and balloons: New results and PDS archive. Icarus 305, 277–283.
320 https://doi.org/10.1016/j.icarus.2017.12.044

321 Marcq, E., Bertaux, J.-L., Montmessin, F., and Belyaev, D. (2012). Variations of sulfur dioxide at
322 the cloud top of Venus's dynamic atmosphere. Nature Geoscience 6, 25–28.
323 https://doi.org/10.1038/ngeo1650

324 Mueller, N. et al. (2008). Venus surface thermal emission at 1 μm in VIRTIS imaging
325 observations: evidence for variation of crust and mantle differentiation conditions. JGR 113,
326 E00B17. https://doi.org/10.1029/2008JE003118

327 Pettengill, G.H., Ford, P.G., Johnson, W.T.K., Raney, R.K., and Soderblom, L.A. (1991).
328 Magellan: Radar performance and data products. Science 252, 260–265.
329 https://doi.org/10.1126/science.252.5003.260

330 Rausch, E.O. (1976). Dielectric properties of chlorapatite. Georgia Institute of Technology, p. 268.

331 Rupprecht, G., and Bell, R.O. (1964). Dielectric constant in paraelectric perovskites. Physical
332 Review 135, 748–752. https://doi.org/10.1103/PhysRev.135.A748

Schaefer, L., and Fegley, B. (2004). Heavy metal frost on Venus. Icarus 168, 215–219. https://doi.org/10.1016/j.icarus.2003.11.023

Seiff, A. (1987). Further information on structure of the atmosphere of Venus derived from the VEGA Venus Balloon and Lander mission. Adv. Space Res. 7, 323–328. https://doi.org/10.1016/0273-1177(87)90239-0

Sempich, J., Filiberto, J., and Treiman, A.H. (2020). Venus: A phase equilibria approach to model surface alteration as a function of rock composition, oxygen- and sulfur fugacities. Icarus 346, 113779. https://doi.org/10.1016/j.icarus.2020.113779

Shalygin, E.V., et al. (2015). Active volcanism on Venus in the Ganiki Chasma rift zone. GRL 42, 4762–4769. https://doi.org/10.1002/2015GL064088

Shepard, M.K., Arvidson, R.E., Brackett, R.A., and Fegley, B. (1994). A ferroelectric model for the low emissivity highlands on Venus. GRL 21, 469–472. https://doi.org/10.1029/94GL00392

Smrekar, S.E, Hensley, S., Dyar, D., and Helbert, J. (2020). VERITAS (Venus emissivity, radio science, InSAR, Topography and spectroscopy): A proposed discovery mission. 51st LPSC Abstracts, 1449.

Teffeteller, H., et al. (2022). An experimental study of the alteration of basalt on the surface of Venus. Icarus, 115085, https://doi.org/10.1016/j.icarus.2022.115085

Treiman, A.H., Harrington, E., and Sharpton, V. (2016). Venus' radar-bright highlands: Different signatures and materials on Ovda Regio and on Maxwell Montes. Icarus 280, 172–182. http://dx.doi.org/10.1016/j.icarus.2016.07.001

353 **Table(s)**

354 Table 1 – Values for the seven sites of interest in Ganis Chasma. Sites 1–4 correspond to the
355 locations of the VMC thermal anomalies indicated in Shalygin et al. (2015). Sites 5–7 are control
356 areas with similar morphology and altitude range to sites 1–4.

Sites	Features	Lon. (°E)	Lat. (°N)	Area (km^2)	Minimum emissivity	Altitude (km)	Temp. (K) (*)	Excursion magnitude (%)
1	VMC anomaly	12.5	197.6	23300	0.718	6055.4	704.6	15.5
2	VMC anomaly	16.5	197.6	31100	0.672	6055.4	704.6	20.9
3	VMC anomaly	18.2	191.5	31700	0.718	6055.8	700.7	15.5
4	VMC anomaly	12.0	199.3	38200	0.753	6054.2	715.6	11.4
5	Control area	20.1	187.3	34440	0.595	6056.2	696.5	30.0
6	Control area	17.4	194.6	12200	0.684	6055.4	704.6	19.5
7	Control area	16.2	193.9	54600	0.600	6054.5	712.9	29.4
Notes: (*) Temperatures are derived from extrapolation of the Vega 2 lander data (Seiff, 1987; Lorenz et al., 2018) and reported in Brossier et al. (2020).								

357

Figure Captions [2-column for all figures, and color should be used online only]

Figure 1 – Ganis Chasma (192°E, 18°N) showing Magellan SAR image (gray scale) and the main morphologic features. The seven sites of interest are outlined in red. Morphologic features are mapped after Ivanov and Head (2011): Ganis Chasma (rift zone), Sitwell crater (with its parabola), Bathkirtseff crater, Yolkai-Estsan Mons, and surrounding tesserae. Maps (here and in Figure 2) have a simple cylindrical projection and north is up. Magellan images covering the study area and shapefiles (and auxiliary files) for the mapped units and sites of interest can be found in the online repository linked to this work (Brossier et al. 2022).

Figure 2 – Magellan radar emissivity and elevation overlapping SAR image (same as Figure 1) at Ganis Chasma (192°E, 18°N): (A) radar emissivity varies from low values in blue to high values in red, while (B) elevation varies from low elevations in teal to high elevation areas in brown.

Figure 3 – (A) Elevation vs emissivity plots obtained for the studied sites. Vertical lines in plots are reference values of emissivity at 0.7 (continuous) and 0.8 (dashed). (B) Magnitude of emissivity excursions (percent change from global average value of 0.85) detected in each site vs. corresponding altitude and temperature. Temperatures are given by the Vega 2 lander data (Seiff, 1987; Lorenz et al., 2018; Brossier et al., 2020). Elevation (as planetary radius, in km) and emissivity values are reported as text files in the online repository (Brossier et al., 2022).

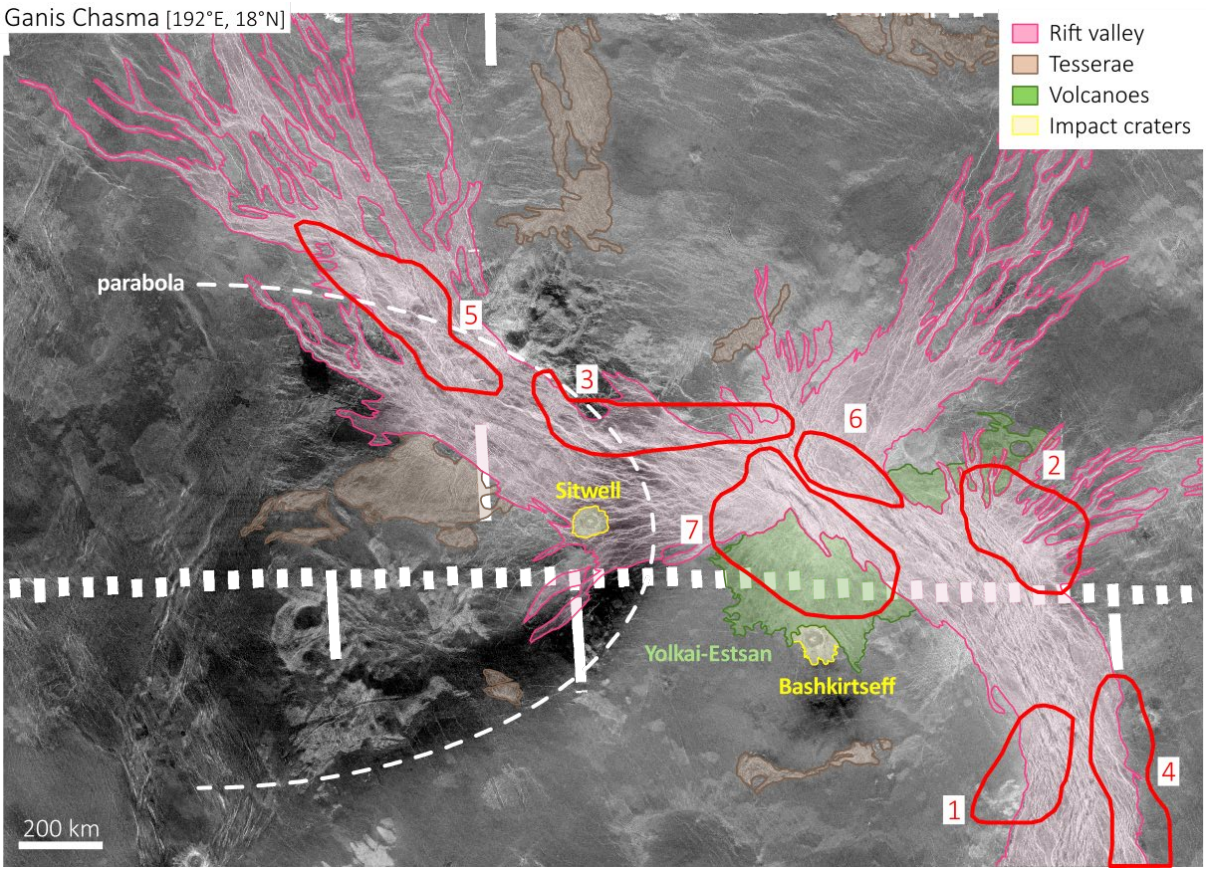
Ganis Chasma [192°E, 18°N]
Rift valley
Tesserae
Volcanoes
Impact craters
parabola
5
3
6
2
Sitwell
7
Yolkai-Estsan
Bashkirtseff
4
1
200 km

Figure 1

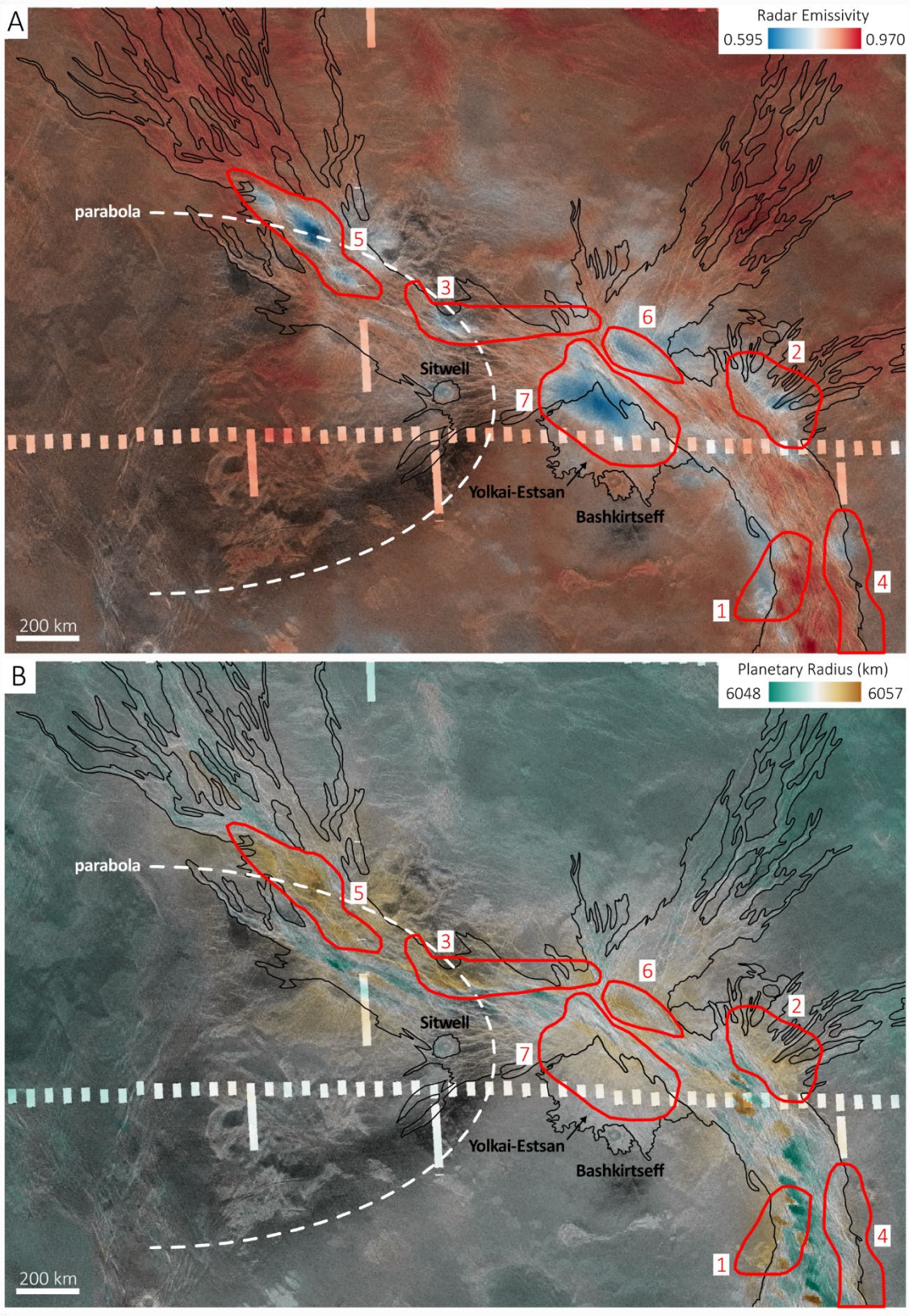
A
Radar Emissivity
0.595
0.970
parabola
5
3
6
2
Sitwell
7
Yolkai-Estsan
Bashkirtseff
1
4
200 km
B
Planetary Radius (km)
6048
6057
parabola
5
3
6
2
Sitwell
7
Yolkai-Estsan
Bashkirtseff
1
4
200 km

Figure 2

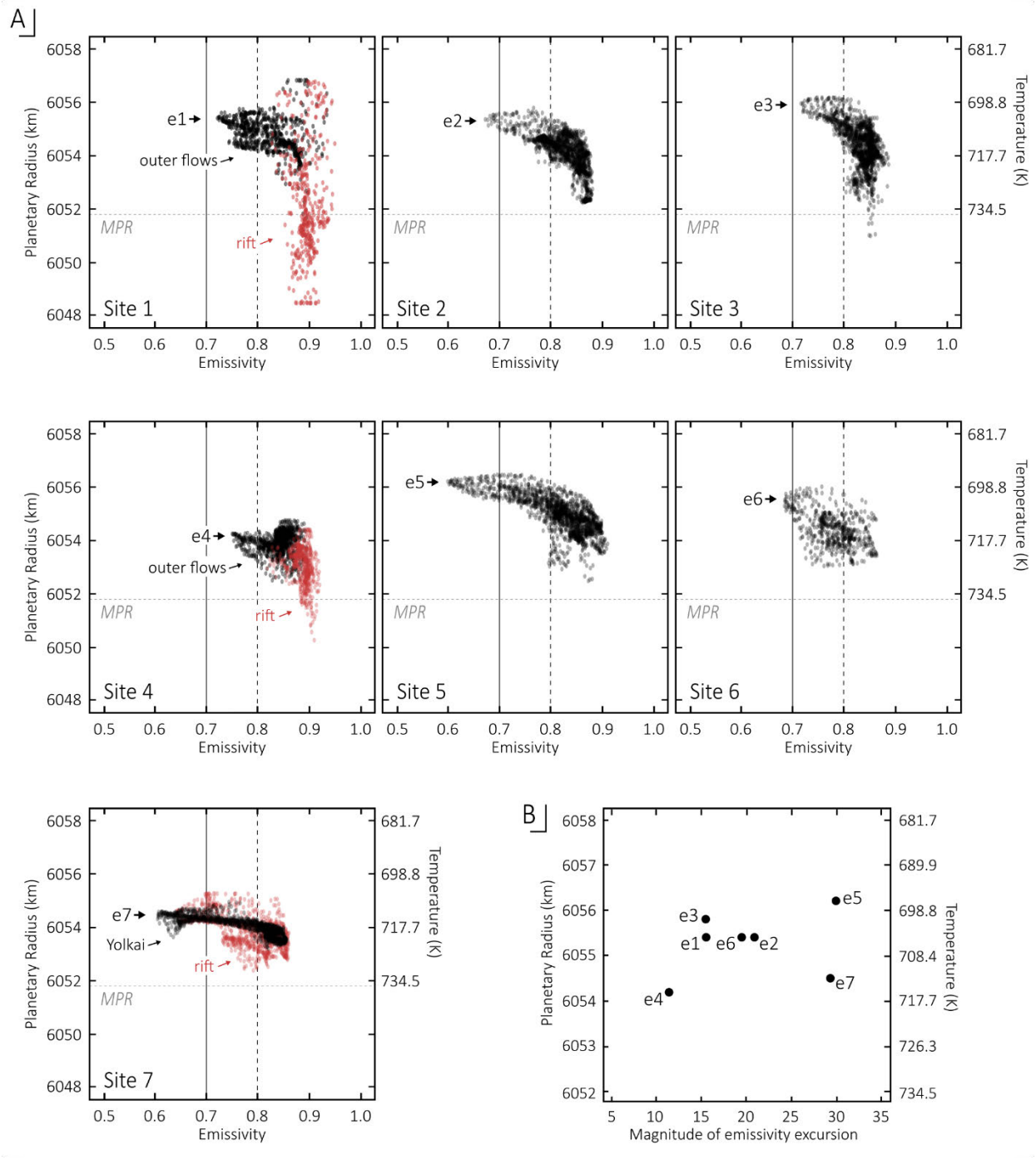

379

380 Figure 3